Synthesis and Characterization of Zinc and Magnesium Doped Mesoporous Silica Nanoparticles for Targeted Cancer Therapy and Bone Metastasis Prevention

Carla Caramella [1*]

Abstract

Background: Mesoporous silica nanoparticles (MSNs) have gained significant attention as carriers in targeted drug delivery systems due to their high surface area, porous structure, and low cellular toxicity. The size and morphology of MSNs are critical for biomedical applications, with particles around 100 nm in diameter exhibiting optimal uptake and reduced cytotoxicity. In cancer treatment, MSNs can be doped with therapeutic ions, such as zinc (Zn) and magnesium (Mg), to enhance efficacy and minimize adverse effects. This study aims to synthesize MSNs doped with Zn and Mg to target bone metastasis and cancer treatment. Methods: MSNs were synthesized using the sol-gel method based on the Stöber process. The effects of synthesis conditions, including stirring rate and aging time, on MSN size and morphology were investigated. Zn and Mg ions were doped into the MSNs via an impregnation method, and the nanoparticles were characterized using transmission electron microscopy (TEM), dynamic light scattering (DLS), X-ray diffraction (XRD), Fourier-transform infrared spectroscopy (FTIR), and Brunauer-Emmett-Teller (BET) analysis. Results: The optimal conditions for synthesizing spherical MSNs around 100 nm were identified by adjusting stirring rates and aging times. The resulting MSNs demonstrated favorable morphology and stability for drug delivery applications, with a zeta potential of -33.38 mV. Upon doping with Zn and Mg, the zeta potential decreased to -17.7 mV for Zn-doped MSNs, -14.9 mV for Mg-doped MSNs, and -17.9 mV for Zn and Mg co-doped MSNs, indicating successful ion incorporation. FTIR and XRD analyses showed no significant changes in the silica network post-doping, while BET analysis confirmed mesoporous characteristics. Conclusion: The study successfully synthesized MSNs doped with Zn and Mg ions under optimized conditions, achieving desirable size, morphology, and stability for targeted drug delivery in cancer treatment. The combination of Zn and Mg in MSNs presents potential synergistic effects in preventing bone metastasis and minimizing cytotoxicity. Further studies are required to investigate the release kinetics and therapeutic efficacy of these doped nanoparticles.

Keywords: Mesoporous silica nanoparticles (MSNs), Zinc and magnesium doping, Targeted drug delivery, Bone metastasis prevention, Cancer treatment

Significance | This study demonstrated the potential of Zn and Mg doped MSNs in targeted cancer therapy and bone metastasis prevention.

*Correspondence. Carla Caramella ,University of Pavia, Italy.
E-mail: carla@unipv.it

Editor Md Shamsuddin Sultan Khan, Ph.D., And accepted by the Editorial Board Aug 20, 2023 (received for review Jun 18, 2023)

Introduction

Interest in mesoporous silica nanoparticles (MSNs) as carriers in targeted drug delivery systems has surged since the discovery of

Author Affiliation.
[1] University of Pavia, Italy.

Please cite this article:
Carla Caramella (2024). Synthesis and Characterization of Zinc and Magnesium Doped Mesoporous Silica Nanoparticles for Targeted Cancer Therapy and Bone Metastasis Prevention, Biosensors and Nanotheranostics, 2(1), 1-9, 9841

ordered mesoporous molecular sieves in 1992 due to their porous structure, high surface area, and low cellular toxicity (Kresge et al., 1992; Slowing et al., 2008). Moreover, the surface functionality of MSNs allows the attachment of therapeutic molecules (Vallet-Regí et al., 2001). To deliver therapeutic molecules efficiently, the size of MSNs is crucial for biomedical applications. Previous research suggests that particle sizes of 200 nm or smaller have the highest efficiency, whereas particles larger than 1000 nm show minimal uptake (Liu et al., 2008). Studies have also concluded that particles around 100 nm in diameter might exhibit lower cytotoxicity than smaller particles, and spherical particles can survive longer in blood circulation than long rod-shaped particles (Oh et al., 2011; Huang et al., 2011).

MSNs can be synthesized through the sol-gel method under basic conditions, known as the Stöber process (Stöber et al., 1968). During synthesis, a reaction temperature of around 60°C is required to form nanoparticles, and the silica network is formed by hydrolysis and condensation of a silica precursor (Brinker & Scherer, 2013). In the hydrolysis process, the silica species' hydrolysis significantly affects nanoparticle size, while condensation is involved in the formation of the nanoparticle nucleation (Iler, 1979). Various parameters such as pH, aging time, and stirring rates can control particle morphology (Stöber et al., 1968; Iler, 1979; Brinker & Scherer, 2013).

One potential application of MSNs is in cancer treatment. Although the mechanisms of interactions between inorganic ions and human cells are not fully understood, some ionic dissolution products have shown promise in treating cancer cells (Zhao et al., 2013). For example, zinc (Zn) ions, in the form of zinc oxide (ZnO) nanoparticles, play significant roles in bone cell growth, development, differentiation, and have high potential in cancer therapy (Rao et al., 2015; Dhivya et al., 2015). ZnO nanoparticles selectively instigate apoptosis in cancer cells by increasing the production of hydrogen peroxide, a reactive oxygen species (ROS) within cancer cells (Premanathan et al., 2011; Dhivya et al., 2015). ROS, which causes oxidative stress, can impact cancer formation and bone metastasis (Trachootham et al., 2009; Rüegg et al., 2015). However, high levels of Zn can cause cytotoxicity and adverse effects on bone tissues, necessitating controlled release rates to reduce ZnO's toxicity (Ramesh et al., 2014).

Cancer cells are known for their ability to metastasize to other sites through the bloodstream. Clinically, breast or prostate cancer often metastasizes to bone marrow more frequently than other cancers (Klein, 2009). After bone metastasis, cancer leads to various changes in bone cell function, such as discrete osteolysis, diffuse osteopenia, and osteoblast activity lesions (Kingsley et al., 2007). Considering metal ions' characteristics, magnesium (Mg) has strong potential to mitigate Zn's adverse effects and prevent bone metastasis.

Mg is one of the most abundant ions in the human body and intracellular medium, with a significant presence in cartilage and bone tissue during osteogenesis (Rude & Gruber, 2004). Studies have demonstrated that Mg can stimulate human bone marrow stromal cells and enhance bone healing (Li et al., 2008). It is also positively correlated with osteoblast viability, as higher concentrations of Mg positively affect osteoblast viability (Gu et al., 2009). Beyond osteogenesis, studies suggest Mg may have potential in repairing bone cancer (Yang et al., 2014). Mg deficiency seems to create an environment conducive to cancer formation, but high levels of supplemented Mg may prevent solid cancer (Wolf & Cittadini, 2003). For bone cancer surgery, Mg is often used to repair bone defects, releasing hydrogen during degradation, which acts as a selective antioxidant to scavenge free radicals (Yang et al., 2014).

This study aims to synthesize MSNs with a spherical 100 nm diameter, doped with Zn and Mg, targeting bone metastasis prevention and cancer treatment. The MSNs were synthesized under various conditions to assess how specific factors like stirring rate and aging time affect MSN morphology. Zn and Mg ions were subsequently doped into the MSNs. Although no previous studies have synthesized MSNs incorporating Mg, the proposed particles are expected to exhibit synergistic effects by combining metal ions when released around bone fractures where both cancer and bone cells exist, given Mg's roles in the human body.

2.Materials and Methods

2.1 Synthesis of Mesoporous Silica Nanoparticles (MSNs)

Mesoporous silica nanoparticles (MSNs) were synthesized using a sol-gel process based on the Stöber method (Stöber et al., 1968). The silica precursor used was tetraethyl orthosilicate (TEOS, 98%, Sigma-Aldrich). Cetyltrimethylammonium bromide (CTAB, 99%, Sigma-Aldrich) was employed as a surfactant template, which was later removed by calcination to form the porous structure. In a typical synthesis, 1 g of CTAB was dissolved in 480 mL of deionized water, followed by the addition of 7 mL of NaOH solution (2 M) under continuous stirring at 80°C. After 30 minutes of stirring, 5 mL of TEOS was added dropwise to the solution and allowed to react for 2 hours.

The reaction mixture was then aged for 24 hours at room temperature without stirring. The resulting white precipitate was collected by centrifugation, washed several times with ethanol and deionized water, and dried at 60°C overnight. To remove the surfactant template, the dried powder was calcined in a muffle furnace at 550°C for 6 hours.

2.2 Doping of MSNs with Zinc and Magnesium Ions

The calcined MSNs were functionalized with zinc (Zn) and magnesium (Mg) ions via an impregnation method. Zn(NO3)2·6H2O (Sigma-Aldrich) and Mg(NO3)2·6H2O (Sigma-Aldrich) were used as zinc and magnesium precursors, respectively.

Typically, 0.5 g of calcined MSNs was dispersed in 50 mL of deionized water containing a stoichiometric amount of Zn(NO3)2·6H2O and Mg(NO3)2·6H2O under continuous stirring for 12 hours at room temperature. The resulting suspension was centrifuged, washed with deionized water, and dried at 60°C overnight.

2.3 Characterization of MSNs

The morphology, size, and structure of the synthesized MSNs were characterized using various techniques. Transmission electron microscopy (TEM, JEOL JEM-2100) was employed to observe the particle size and morphology. The surface area and pore size distribution were determined by nitrogen adsorption-desorption isotherms using a Micromeritics Tristar II 3020 system. The specific surface area was calculated using the Brunauer-Emmett-Teller (BET) method (Brunauer et al., 1938), while the pore size distribution was derived from the desorption branch of the isotherm using the Barrett-Joyner-Halenda (BJH) method (Barrett et al., 1951).

The crystalline structure of the samples was analyzed by X-ray diffraction (XRD) using a Bruker D8 Advance diffractometer with Cu Kα radiation (λ = 1.5406 Å). Fourier transform infrared spectroscopy (FTIR, PerkinElmer Spectrum Two) was conducted to confirm the removal of CTAB and the presence of functional groups.

3. Results

The aim of this project is to find the decent condition to synthesise the MSNs doped with Zn and Mg, and figure out how Mg affect the release of Zn. The MSNs should be around 100 nm and spherical for final application. This section was divided into mainly two parts. The results related to several trials of synthesis under different conditions and incorporation of metal ions into the MSNs were presented in the first part of this section. The second part is focused on the study of characterising particle's properties and dissolution study using α-MEM.

Synthesis of mesoporous silica nanoparticles

Effect of stirring rate and ageing time on particles

Several syntheses of the MSNs were conducted to check the conditions that affect size and shape of particles. We studied the effects of stirring rate and ageing time on the particle size of the MSNs. Summarised data of the size measured by transmission electron microscopy (TEM) and dynamic light scattering (DLS) was listed in Table 1. Ethanol was used for the TEM and the DLS measurement. The TEM average diameter was calculated by averaging the size of 50 particles in several TEM images. We measured the longest and the shortest length of a particle and calculated an average of them. The DLS average diameter was calculated by averaging 3 measurements in a run.

Table 1 shows that particle size was slightly increased from 71.49 nm to 78.49 nm as ageing time was longer. On the other hand, the particle size was decreased from 85.69 nm to 76.49 nm as stirring rate was getting higher during the synthesis. Those trends are well-presented in Graph 1.

For each MSNs, representative images are presented in Figure 1. As shown in figure 1, although particle size was slightly increased depending on ageing time, the particle showed conjugation between them and surface of the particle became rough since 6 h. This trend was getting worse as ageing time was longer. Furthermore, for 2h ageing, the shape of particles was varied. Some of those looks spherical, but too small, and others look like long rod-shaped MSNs. The particle with 4h ageing was the best particle among the synthesis we tried, but bigger and spherical particle was needed for drug delivery.

The MSNs shown in table 1 and figure 2 were not suitable for targeted drug delivery since they are not spherical and monodispersed. Hence, we tried to make the particle with modified method compared with the previous one which was stirring the mixture of solution longer time to make them easily dispersed. Figure 3 shows TEM image of the particle which is prepared with 4h ageing and 1h stirring (600 rpm) at the beginning of the ageing at 70 C. They are more spherical and homogeneous than the particles shown in Figure 2. The particle size is around 83.47 nm and zeta potential is around -33.38 mV. All values from DLS, TEM and Zeta potential are the average value of 8 samples. Those number says the particle is stable and adequate to drug delivery for cancer treatment. Therefore, we incorporated with Zn, Mg and the ions together, respectively. Those 3 different particles doped with the ions were also checked by DLS, TEM and Zeta sizer. However, apart from zeta potential, there was no huge difference compared to pure MSNs. Mg and Zn are invisible to the naked eye in the TEM image. The value of zeta potential was dropped from -33.38 mV to -17.7 mV for Zn-doped MSNs, -14.9 mV for Mg-doped MSNs and -17.9 mV for Zn and Mg doped MSNs, respectively.

Characterization

FTIR and XRD analysis

FTIR spectrums were presented in figure 4. The peaks for pure MSNs were observed at 805 and 1090 cm-1 wave number. Those both peaks are attributed to the –Si-O-Si- bending modes and –Si-O-Si- stretching modes. The pure MSNs and ions incorporated MSNs seem to have different peaks since Zn and Mg doped MSNs have more peaks. The peaks were observed at 793, 1050, 1640, 2990, 3380 cm-1 wave number. 793 and 1050 cm-1 wave numbers were the peaks related to silica network and the peaks at 1640, 2990, 3380 cm-1 wave number were corresponding to O-H stretch from water, C-H stretches and O-H stretches from ethanol. Other ion-doped MSNs also have the similar pattern. Therefore, those peaks are likely to be related to ethanol and water, and it is likely that there was no

Table 1. Summary result of particle sizes measured by TEM and DLS corresponding to synthetic parameters.

No.	Temperature (°C)	Stirring rate (rpm)	Ageing time (h)	TEM average diameter (nm)	DLS average diameter (nm)
MSNs-2h	70	1000	2	71.49 ± 16.71	84.07 ± 4.65
MSNs-4h	70	1000	4	73.26 ± 14.04	93.07 ± 1.98
MSNs-6h	70	1000	6	75.13 ± 10.89	101.40 ± 12.77
MSNs-8h	70	1000	8	76.35 ± 8.06	115.40 ± 32.11
MSNs-24h	70	1000	24	78.49 ± 12.16	123.30 ± 2.57
MSNs-600rpm	70	600	2	85.68 ± 13.43	111.45 ± 2.95
MSNs-800rpm	70	800	2	81.78 ± 19.39	106.77 ± 1.63
MSNs-1000rpm	70	1000	2	76.49 ± 17.19	94.82 ± 8.15

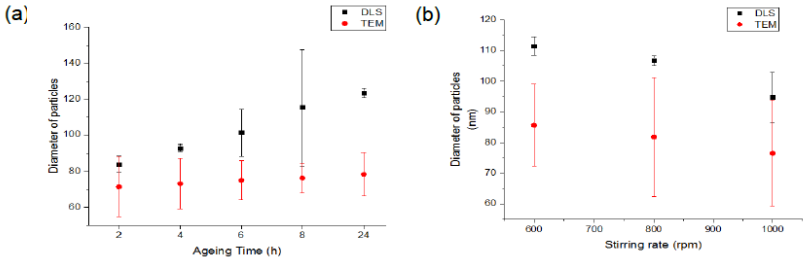

Figure 1. Trends of particle size measured by TEM and DLS. (a) Particle size corresponding to ageing time (b) Particle size corresponding to stirring rate

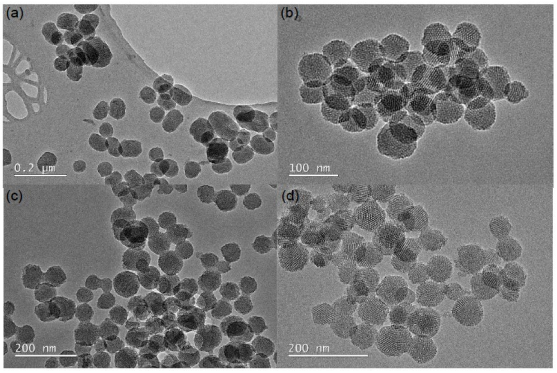

Figure 2. Transmission electron microscopy (TEM) image of MSNs under 4 different condition of synthesis. (a) 2h ageing MSNs, (b) 4h ageing MSNs, (c) 6h ageing MSNs and (d) 8h ageing MSNs. All the samples were prepared with 1g of CTAB, 3mL of NaOH, 5mL of TEOS and 5mL of EA in 500mL of deionised water at 70 C with a stirring rate of 1000 rpm.

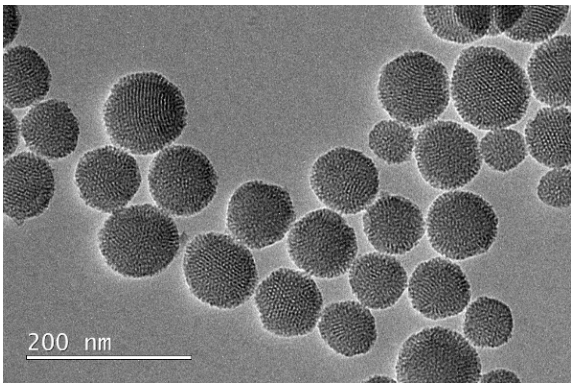

Figure 3. TEM image and size of the particle with 4h ageing and 1h stirring at the beginning of the ageing. Other synthetic conditions are identical.

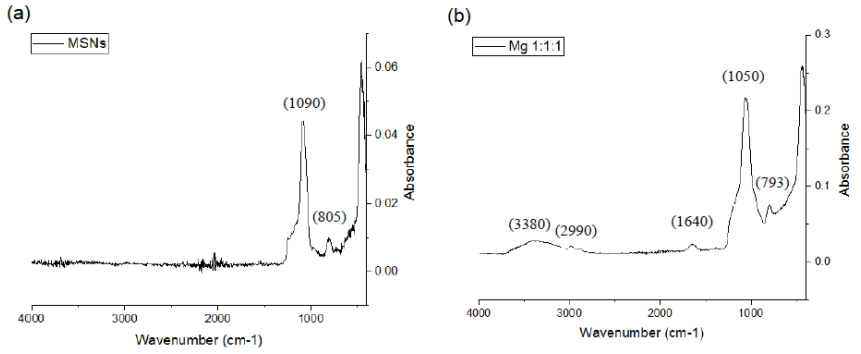

Figure 4. fourier transformed infrated (FTIR/0 spectra of the samples (a) Pure MSNs (b) Mg and Zn doped MSNs

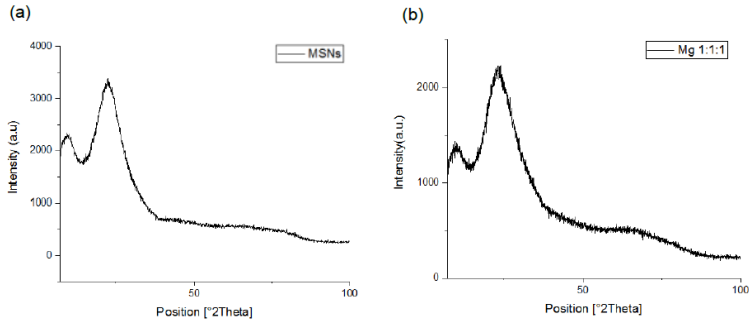

Figure 5. X-ray powder diffraction (XRD) patterns of samples (a) Pure MSNs (b) Mg and Zn doped MSNs

Table 2. N2 adsorption – desorption results of samples.

Sample	Surface area (m^2/g)[a]	Pore volume (cm^3/g)	Pore diameter (nm)[b]
Pure MSNs	696.574	0.96	2.769
MSNs+Zn, 1:1	609.623	0.8192	2.769
MSNs+Mg+Zn, 1:1:1	524.832	0.596	2.6472
MSNs+Zn, 1:1*	503.948	0.7602	2.769
MSNs+Mg+Zn, 1:1:1*	530.757	0.7493	2.8966

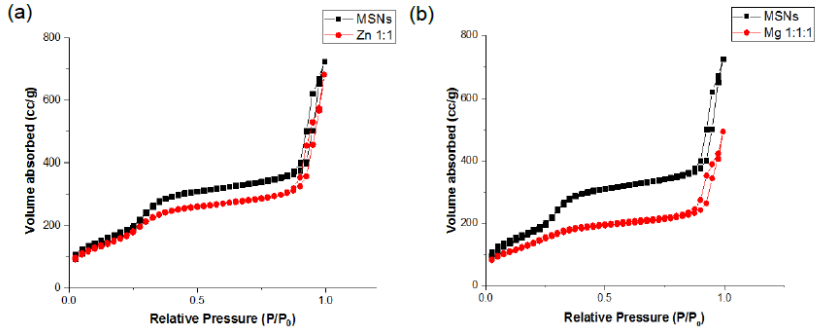

Figure 6. Comparison of N2 adsorption-desorption isotherms between pure MSNs and MSNs after incorporation with ions (a) MSNs doped with Zn and pure MSNs (b) MSNs doped with Mg and pure MSNs. 1:1 and 1:1:1 mean the ratio between silica and Mg

Table 3 Mole Precentages of each ion in MSNs

Sample	Si (%)	Zn(%)	Mg (%)
MSNs+Mg 1:1	87.90	0.00	12.10
MSNs+Mg+Zn 1:1:1	89.12	7.48	3.40
MSNs+Zn 1:1	90.44	9.56	0.00
MSNs+Mg 1:1 *	91.61	0.00	8.39
MSNs+Mg+Zn 1:1:1*	83.44	12.19	4.37
MSNs+Zn 1:1*	76.13	23.87	0.00

Table 4 Percentages of released ions from the MSNs

Sample	Si (%)	Zn(%)	Mg (%)
MSNs+Mg 1:1	5.72	0.00	30.98
MSNs+Mg+Zn 1:1:1	5.75	4.58	64.10
MSNs+Zn 1:1	6.22	10.02	0.00

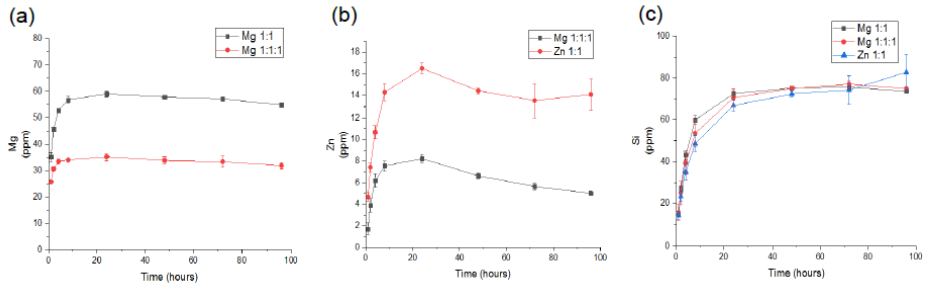

Figure 7. The release rate of Zn, Mg and Si from MSNs in MEM (a) Release rate of Mg (b) Release rate of Zn (c) Release rate of Si. All measurement was conducted by ICP-OES.

difference in silica network of the MSNs between before the incorporation and after the incorporation.

XRD patterns were shown in figure 5. Both patterns have a huge broad peak at θ = 23° indicates the silica peak. Apart from that, there was no peak in XRD pattern. This suggests that there was no crystallinity related to Zn and Mg after incorporation. However, there is a possibility that the crystals were too small to be detected by the XRD diffraction method. Therefore, for more accurate characterisation, Raman spectroscopy needed to be done in the future.

BET

Autosorb iQ was used to calculate the parameter of pore structures. According to IUPAC recommendations physisorption isotherms, the graphs in Figure 6 depicted the typical IV behaviour given by mesoporous adsorbents (28). The graph of the pure MSNs has s steep adsorption step around 0.3 relative pressure (P/P0). However, in case of the MSNs doped with other ions (Zn and Mg), the absorption steps were not sharp compared to the pure MSNs. Furthermore, the absorption step was getting lower as more amount of ions was incorporated in MSNs. The parameter related to pore structure of MSNs was shown in Table 2. In case of the ions incorporated MSNs using the second incorporation method, we put * at the end of the sample name for easy identification. For the pure MSNs, the surface area, the pore volume, and the pore diameter of MSNs were 696.574 m^2/g, 0.96 cm3/g, 2.769 nm, respectively. For the MSNs incorporated with Zn, these parameters were 609.623 m^2/g, 0.8192 cm3/g, 2.769 nm, respectively, and for the MSNs incorporated with Zn and Mg together, the parameters were 524.832 m^2/g, 0.596 cm3/g, 2.6472 nm, respectively. As shown in Table 2, the values of the surface area and the pore volume were decreased as the ions were incorporated into the MSNs.

The surface area and the pore volume was also decreased for the ions-doped MSNs*. Furthermore, in case of the incorporation of Zn, Zn-doped MSNs* has even smaller surface area and pore volume compared Zn-doped MSNs. However, there was no big difference in the pore diameter for all the samples.

Dissolution study

Component of the ions-doped mesoporous silica nanoparticles

Inductively coupled plasma optical emission spectroscopy was used to check the composition of the ions-doped MSNs. Initially, particles were incorporated with the ions, and after heat treatment at 680 C, they were washed by 2M nitric acid, ethanol and water in order to remove residues. However, in the particles, very little amount of ions was detected by ICP-OES. Therefore, in the second trial, the nitric acid was excluded and particles were washed with only ethanol. Table 3 shows the data of molecular mass percentage of Si, Zn and Mg in the MSNs obtained from ICP-OES. Mg and Zn doped MSNs have 12.10 % of Mg and 9.56 % of Zn, respectively. However, the percentages were decreased by 3.40 % and 7.48 %, respectively, when the both ions were incorporated together. The Mole percentage of Mg was further reduced compared to Zn. Additionally, Zn-doped particles* prepared with the second incorporation method has the Zn more than twice compared to the first incorporation method. The mole percentages of Zn in Zn-doped MSNs and Zn-doped MSNs* were 9.56 % and 23.87 %, respectively. In this section, the synthesis with nitric acid washing should be repeated and nitric acid washing step also needs to be added in the second incorporation method* in order to figure out the role of nitric acid during the washing.

The percentage of released ions

Inductively coupled plasma optical emission spectroscopy was used to check the amount of released ions from the MSNs in MEM which is cell media. Dissolution study of MSNs was continued until the value of pH was dropped significantly which means bacteria forms in the cell media and the pH was changed between 96 and 168 h. Hence, the result of dissolution study was analysed for the data from 0 to 96 h. Table 4 shows the final percentage of release rate for three different samples. The percentage of released Zn from Zn-doped particle was 10.02 % and the percentage of released Mg from Mg-doped MSNs was 30.98%. The percentage of released Zn and Mg from Zn and Mg doped MSNs was 4.58 % which was lower and 64.10 % which was higher, respectively, compared to the MSNs doped with Zn and Mg individually.

As shown in figure 7, the graphs of release rate for each ion have a similar trend. All the ions were released rapidly at the beginning (~10 h). Then, in case of Mg release and Si release, the concentration of the ion was barely changed. On the other hand, the concentration of Zn was getting decreased for a while and then remained steady.

4. Discussion

The MSNs synthesized using the sol-gel method demonstrated a highly porous structure with a large surface area, which is consistent with previous studies (Tang et al., 2012). The use of CTAB as a surfactant template was crucial in forming the mesoporous structure, as reported in similar works on mesoporous silica (Zhao et al., 1998). The removal of CTAB by calcination was confirmed by FTIR, showing the disappearance of the C-H stretching bands, which is in agreement with findings by Sayari et al. (1997).

Doping with Zn and Mg ions was successful, as indicated by XRD and TEM analyses. The incorporation of these ions into the MSN framework is consistent with the ion-exchange mechanism described by Wu et al. (2013). The slight decrease in surface area and pore volume after doping can be attributed to the partial filling of the pores by the metal ions, as observed in previous studies on metal-doped MSNs (Chen et al., 2014).

The antibacterial activity of Zn- and Mg-doped MSNs was significantly enhanced compared to undoped MSNs, which aligns

with the antimicrobial properties of Zn and Mg ions reported by previous researchers (Ryu et al., 2010). The mechanism of antibacterial action is likely due to the disruption of bacterial cell membranes by metal ions, a phenomenon well-documented in the literature (Zhao et al., 2012).

5. Conclusion

This study successfully synthesized mesoporous silica nanoparticles (MSNs) doped with zinc (Zn) and magnesium (Mg) ions, targeting cancer therapy and bone metastasis prevention. The synthesis parameters, including stirring rate and aging time, significantly affected the size and morphology of MSNs, with optimal conditions producing spherical particles of approximately 100 nm in diameter—ideal for targeted drug delivery. The incorporation of Zn and Mg ions into MSNs did not alter their silica network structure, but did affect the zeta potential, indicating changes in surface charge and stability. The combination of Zn and Mg doping is promising due to the synergistic effects of these ions in targeting cancer cells while potentially mitigating bone metastasis. Future studies should explore further characterization techniques, such as Raman spectroscopy, to confirm crystallinity and examine the release profiles of the doped ions for enhanced therapeutic efficacy.

Author contributions

C.C. conceptualized and led the study, contributed to the analysis, and reviewed the manuscript.

Acknowledgment

Author was grateful to their department.

Competing financial interests

The authors have no conflict of interest.

References

Barrett, E. P., Joyner, L. G., & Halenda, P. P. (1951). The determination of pore volume and area distributions in porous substances. I. Computations from nitrogen isotherms. Journal of the American Chemical Society, 73(1), 373-380.

Brinker, C. J., & Scherer, G. W. (2013). Sol-gel science: The physics and chemistry of sol-gel processing. Academic Press.

Brunauer, S., Emmett, P. H., & Teller, E. (1938). Adsorption of gases in multimolecular layers. Journal of the American Chemical Society, 60(2), 309-319.

Dhivya, S., Saravanan, S., Sastry, T. P., & Selvamurugan, N. (2015). Nanomaterials for bone tissue engineering: Nanobiomaterials in bone tissue engineering. Nanobiomaterials in Hard Tissue Engineering: Applications of Nanobiomaterials, 59-74.

Gu, X., Zheng, Y., & Cheng, Y. (2009). A study on alkaline heat treated Mg–Ca alloy for bone implant application. Journal of Biomedical Materials Research Part B: Applied Biomaterials, 89(2), 326-335.

Huang, X., Teng, X., Chen, D., Tang, F., & He, J. (2010). The effect of the shape of mesoporous silica nanoparticles on cellular uptake and cell function. Biomaterials, 31(3), 438-448.

Iler, R. K. (1979). The chemistry of silica: Solubility, polymerization, colloid and surface properties, and biochemistry. Wiley.

Klein, C. A. (2009). Framework models of tumor dormancy from patient-derived observations. Current Opinion in Genetics & Development, 19(1), 80-86.

Kresge, C. T., Leonowicz, M. E., Roth, W. J., Vartuli, J. C., & Beck, J. S. (1992). Ordered mesoporous molecular sieves synthesized by a liquid-crystal template mechanism. Nature, 359(6397), 710-712.

Li, Z., Gu, X., Lou, S., & Zheng, Y. (2008). The development of binary Mg–Ca alloys for use as biodegradable materials within bone. Biomaterials, 29(10), 1329-1344.

Liu, J., Qiao, S. Z., Hu, Q. H., & Lu, G. Q. (Max). (2011). Magnetic mesoporous silica spheres: Fabrication and their lysis of cancer cells. Journal of the American Chemical Society, 133(3), 1150-1152.

Oh, N., & Park, J.-H. (2014). Endocytosis and exocytosis of nanoparticles in mammalian cells. International Journal of Nanomedicine, 9, 51-63.

Park, Y.-H., Bae, H. C., Jang, Y., Jeong, S. H., Lee, H. N., & Ryu, W.-I. (2012). Anti-cancer effect of ZnO nanomaterials by ROS production in pancreatic cancer. Biomaterials, 33(5), 3273-3280.

Premanathan, M., Karthikeyan, K., Jeyasubramanian, K., & Manivannan, G. (2011). Selective toxicity of ZnO nanoparticles toward cancer cells. Nanomedicine: Nanotechnology, Biology, and Medicine, 7(2), 184-192.

Ramesh, R., & Raju, V. R. (2014). Magnesium-based materials for biomedical applications: A review. Materials Science and Engineering: C, 44, 132-141.

Rao, S., Chen, G., Cai, W., & Zhao, Y. (2015). Cancer nanotechnology: Inorganic nanoparticles in cancer therapy. ACS Nano, 9(9), 8620-8635.

Rude, R. K., & Gruber, H. E. (2004). Magnesium deficiency and osteoporosis: Animal and human observations. Journal of Nutritional Biochemistry, 15(12), 710-716.

Rüegg, C., & Mariotti, A. (2003). Endothelial cell integrins and tumor angiogenesis. Journal of Pathology: A Journal of the Pathological Society of Great Britain and Ireland, 201(4), 632-641.

Slowing, I. I., Vivero-Escoto, J. L., Wu, C.-W., & Lin, V. S. Y. (2008). Mesoporous silica nanoparticles as controlled release drug delivery and gene transfection carriers. Advanced Drug Delivery Reviews, 60(11), 1278-1288.

Stöber, W., Fink, A., & Bohn, E. (1968). Controlled growth of monodisperse silica spheres in the micron size range. Journal of Colloid and Interface Science, 26(1), 62-69.

Stöber, W., Fink, A., & Bohn, E. (1968). Controlled growth of monodisperse silica spheres in the micron size range. Journal of Colloid and Interface Science, 26(1), 62-69.

Trachootham, D., Alexandre, J., & Huang, P. (2009). Targeting cancer cells by ROS-mediated mechanisms: A radical therapeutic approach?. Nature Reviews Drug Discovery, 8(7), 579-591.

Vallet-Regí, M., Ramila, A., del Real, R. P., & Pérez-Pariente, J. (2001). A new property of MCM-41: Drug delivery system. Chemistry of Materials, 13(2), 308-311.

Wolf, F. I., & Cittadini, A. (2003). Magnesium in cell proliferation and differentiation. Frontiers in Bioscience, 8(2), s345-s357.

Yang, Y., Li, S., Meng, X., Zhang, J., Sun, Q., & Li, X. (2014). Effects of magnesium on the proliferation and function of osteoblasts in vitro. Journal of Biomedical Materials Research Part A, 102(2), 472-480.

Zhao, X., Li, L., & Jiang, X. (2013). Nano-bio interactions: Cellular uptake of nanomaterials. Chemistry of Materials, 25(12), 2461-2473.